

Dimension decomposition algorithm for multiple source localization using uniform circular array

SU Xiaolong¹, HU Panhe^{1,*}, WEI Zhenhua², LIU Zhen¹, SHI Junpeng¹, and LI Xiang¹

1. College of Electronic Science and Technology, National University of Defense Technology, Changsha 410073, China;

2. Combat Support College, Rocket Force University of Engineering, Xi'an 710025, China

Abstract: A dimension decomposition (DIDE) method for multiple incoherent source localization using uniform circular array (UCA) is proposed. Due to the fact that the far-field signal can be considered as the state where the range parameter of the near-field signal is infinite, the algorithm for the near-field source localization is also suitable for estimating the direction of arrival (DOA) of far-field signals. By decomposing the first and second exponent term of the steering vector, the three-dimensional (3-D) parameter is transformed into two-dimensional (2-D) and one-dimensional (1-D) parameter estimation. First, by partitioning the received data, we exploit propagator to acquire the noise subspace. Next, the objective function is established and partial derivative is applied to acquire the spatial spectrum of 2-D DOA. At last, the estimated 2-D DOA is utilized to calculate the phase of the decomposed vector, and the least squares (LS) is performed to acquire the range parameters. In comparison to the existing algorithms, the proposed DIDE algorithm requires neither the eigendecomposition of covariance matrix nor the search process of range spatial spectrum, which can achieve satisfactory localization and reduce computational complexity. Simulations are implemented to illustrate the advantages of the proposed DIDE method. Moreover, simulations demonstrate that the proposed DIDE method can also classify the mixed far-field and near-field signals.

Keywords: source localization, parameter estimation, uniform circular array (UCA), propagator, partial derivative, least squares (LS).

DOI: [10.23919/JSEE.2023.000016](https://doi.org/10.23919/JSEE.2023.000016)

1. Introduction

Source localization plays an important role in array signal processing [1–5], which has important applications in massive multiple input multiple output (MIMO) radar and jamming suppression [6–9]. The near-field sources in space need to be described by direction of arrival (DOA)

and range parameter. In contrast, the far-field sources only need to be described by DOA [10,11]. By applying the orthogonal property of the steering vector and the noise subspace, one-dimensional (1-D) multiple signal classification (MUSIC) method and estimating signal parameter via rotational invariance technique (ESPRIT) method are used to estimate the DOA of far-field sources. Compared with the above methods for estimating incoherent sources [12], the sparse representation method is proposed to achieve the super-resolution estimation of coherent far-field sources [13].

However, the near-field sources locate at the Fresnel region of array and can be considered as spherical wavefront [14–18], and the traditional algorithms with the far-field assumption can not be applied to the near-field source localization [19–23]. Near-field source localization plays an important role for indoor passive detection, underwater acoustic detection, etc. [24–27]. In addition to DOA, the range parameter also needs to be estimated [28–34]. By implementing the structure of uniform linear array (ULA) with the cocentered orthogonal loop and dipole antennas, the theory of rank reduction (RARE) is applied to obtain the joint DOA, range, and polarization of the rectilinear near-field signals (NFSs) [35]. By utilizing the RARE principle [36], DOA and range parameter are separated to solve the nonlinear optimization problem, which can avoid the two-dimensional (2-D) search process. Moreover, a new efficient method in [37] employs the non-Hermitian cumulant matrix to reduce the computational complexity, which requires only one matrix and one eigenvalue decomposition.

Recently, numerous researches focus on the configuration of uniform circular array (UCA) to estimate the 2-D DOA and range parameter of near-field sources. Compared to the configuration of ULA that can only achieve the estimation of 1-D DOA of near-field sources [38], the structure of UCA is an attractive array structure that can be applied to acquire the 2-D DOA (i.e., azimuth angle

Manuscript received March 19, 2021.

*Corresponding author.

This work was supported by the National Natural Science Foundation of China (62022091;61921001).

and elevation angle) [39]. Although the three-dimensional (3-D) MUSIC algorithm in [40] can jointly estimate the 2-D DOA and range parameters of near-field sources, it requires expensive computational cost to search the spectrum peaks. By transforming 3-D localization into 2-D and 1-D parameter estimation, the two-stage MUSIC (TSMUSIC) method in [41] and the second-order statistics (SOS) method in [42] respectively apply the 2-D MUSIC algorithm and the ESPRIT-like algorithm to estimate the 2-D DOA. Yet, both of the above methods employ the 1-D MUSIC algorithm to acquire range parameters. Noticeably, the 1-D MUSIC algorithm needs eigendecomposition and the search process for range estimation, which increases the computational cost. By developing the least squares (LS) to reduce computational complexity, the phase-based algorithms [43–45] were proposed to jointly acquire the 2-D DOA and range parameter of near-field sources. However, the estimation accuracy is lower than the 3-D MUSIC algorithm. By decomposing the steering vector of ULA, the reduced-dimension MUSIC (RDMUSIC) method [46] is proposed to avoid the search process of range spatial spectrum and reduce computational complexity. However, the RDMUSIC method can only estimate the 1-D DOA via ULA. Thus, it can not be directly applied to estimate 2-D DOA via UCA.

In addition, due to the fact that the far-field signal (FFS) can be considered as the state where the range parameter of the NFS is infinite, the algorithm for the near-field source localization is also suitable for estimating the DOA of FFS [47,48]. To be exact, based on whether the calculated range parameter is in the Fresnel area of array, the algorithms for near-field source localization can be applied to classify the mixed near-field and far-field sources [49,50]. In [51], the improved ESPRIT-like method and 1-D MUSIC method were exploited to obtain the spatial spectrum of 2-D DOA and range parameter, where the pure near-field component was extracted from mixed sources by employing covariance differencing method. Noticeably, the propagator was utilized to acquire the noise subspace, which can reduce computational complexity. Moreover, the method in [52] calculated the phase difference of the centro-symmetric sensors to separate the 2-D DOA and range parameter. Since the 2-D DOA of mixed sources was performed by applying the phase-based algorithm, the computational complexity was reduced while the accuracy of estimation was also reduced. However, both of the above methods require the search process for the peaks in the range spatial spectrum, which implies increased computational complexity.

Therefore, the motivation of this work is to achieve satisfactory localization while reducing computational

complexity. Since the FFS can be considered as the state where the range parameter of the NFS is infinite, the algorithm for the near-field source localization can also be utilized to estimate the DOA of far-field sources. In this paper, we propose a dimension decomposition (DIDE) algorithm to achieve 3-D localization by employing the configuration of UCA. By decomposing the first and second exponent term in the steering vector of UCA, we transform 3-D localization into 2-D and 1-D parameter estimation. Firstly, we partition the received data and implement propagator to acquire noise subspace. Then, by constructing the objective function to deal with the optimization problem, we exploit partial derivative to acquire the spatial spectrum of 2-D DOA. Finally, by applying the phase of the decomposed vector, we perform the LS method to estimate the range parameter. The advantage of the proposed DIDE method is that it requires neither the eigendecomposition of covariance matrix nor the search process of range spatial spectrum. Simulation results verify that the proposed DIDE method can achieve the paired 3-D parameter estimation and reduce the computational cost. Moreover, the proposed DIDE method can also achieve the classification of incoherent mixed sources.

2. Signal model

As depicted in Fig. 1, the UCA is impinged by an NFS, which is composed of M omnidirectional sensors with radius R . The near-field area is from $0.62\sqrt{8R^3/\lambda}$ to $8R^2/\lambda$, where λ stands for the source wavelength. We assume that the number of signals K is known in advance. The k th NFS is located at (ϕ_k, θ_k, r_k) in polar coordinate, where azimuth angle ϕ_k is measured from the x -axis, elevation angle θ_k is measured from the z -axis, and range parameter r_k is measured from the center of UCA.

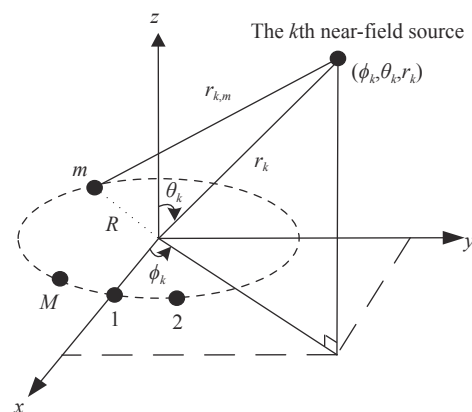


Fig. 1 Structure of UCA with a near-field source

In practice, the received data of the m th sensor at the n th snapshot can be written as

$$x_m(n) = \sum_{k=1}^K s_k(n) e^{j\tau_{k,m}} + w_m(n)$$

$$m = 1, 2, \dots, M; n = 1, 2, \dots, N \quad (1)$$

where N denotes the number of snapshot, $s_k(n)$ denotes the k th signal at the n th snapshot, and $w_m(n)$ denotes the additive complex Gaussian white noise. $\tau_{k,m}$ is determined by

$$\tau_{k,m} = \frac{2\pi}{\lambda} (r_k - r_{k,m}) \quad (2)$$

where $r_{k,m}$ denotes the distance from the k th NFS to the m th sensor, which can be expressed as

$$r_{k,m} = \sqrt{r_k^2 + R^2 - 2r_k R \zeta_{k,m}} \quad (3)$$

In (3), $\zeta_{k,m}$ is calculated as $\cos(\gamma_m - \phi_k) \sin \theta_k$ and γ_m is calculated as $2\pi(m-1)/M$. By employing the second-order Taylor series in [43, 44], $r_{k,m}$ at R/r_k can be expanded as

$$r_{k,m} = r_k - R \zeta_{k,m} + \frac{R^2}{2r_k} (1 - \zeta_{k,m}^2) + O\left(\frac{R^2}{r_k^2}\right) \quad (4)$$

Therefore, the 2-D DOA is split out from the steering vector, and the signal model for the m th sensor can be rewritten as

$$x_m(n) = \sum_{k=1}^K s_k(n) \exp \left[j \left(\frac{2\pi R}{\lambda} \zeta_{k,m} - \frac{\pi R^2}{\lambda r_k} (1 - \zeta_{k,m}^2) \right) \right] + w_m(n) =$$

$$\sum_{k=1}^K s_k(n) \exp [j(\eta_{k,m} - \xi_{k,m})] + w_m(n) \quad (5)$$

where $\eta_{k,m}$ is written as $(2\pi R/\lambda) \zeta_{k,m}$ and $\xi_{k,m}$ is written as $(\pi R^2/\lambda r_k) (1 - \zeta_{k,m}^2)$. Since the exponent term in (5) is performed through the Taylor series expansion, there is an error between the simplified signal model and the actual

received data.

Obviously, when the range parameters exceed the near-field area, the near-field sources can be regarded as far-field sources. Compared with the signal model for near-field source in (5), the signal model for the FFS does not include range parameter r_k and the second exponent term. Thus, the signal model for the far-field source is given by

$$x_m(n) = \sum_{k=1}^K s_k(n) e^{j\eta_{k,m}} + w_m(n) \quad (6)$$

To be specific, the matrix of the received data $\mathbf{X} = [\mathbf{x}(1), \mathbf{x}(2), \dots, \mathbf{x}(N)]$ with $\mathbf{x}(n) = [x_1(n), x_2(n), \dots, x_M(n)]^T$ is given by

$$\mathbf{X} = \mathbf{A}\mathbf{S} + \mathbf{W} \quad (7)$$

where $\mathbf{S} = [s(1), s(2), \dots, s(N)]$ with $s(n) = [s_1(n), s_2(n), \dots, s_K(n)]^T$ denotes the NFS in matrix form, $\mathbf{W} = [\mathbf{w}(1), \mathbf{w}(2), \dots, \mathbf{w}(N)]$ with $\mathbf{w}(n) = [w_1(n), w_2(n), \dots, w_M(n)]^T$ denotes the complex Gaussian white noise in matrix form, $(\cdot)^T$ denotes the transpose operator, and \mathbf{A} denotes the steering matrix of UCA. \mathbf{A} can be expressed as

$$\mathbf{A} = [\mathbf{a}(\phi_1, \theta_1, r_1), \mathbf{a}(\phi_2, \theta_2, r_2), \dots, \mathbf{a}(\phi_K, \theta_K, r_K)] \quad (8)$$

Since the UCA holds the centro-symmetric property, we can acquire $\zeta_{m+M/2} = -\zeta_m$ and $\gamma_{m+M/2} = \gamma_m + \pi$. Hence, we can get $\xi_{k,m+M/2} = \xi_{k,m}$ and $\eta_{k,M/2+m} = -\eta_{k,m}$. Thus, the k th column in (8) is given by

$$\mathbf{a}(\varphi_k, \theta_k, r_k) = [a_{k,1}, \dots, a_{k,M/2}, a_{k,M/2+1}, \dots, a_{k,M}]^T =$$

$$[e^{j\eta_{k,1} - j\xi_{k,1}}, \dots, e^{j\eta_{k,M/2} - j\xi_{k,M/2}}, e^{j\eta_{k,M/2+1} - j\xi_{k,M/2+1}}, \dots, e^{j\eta_{k,M} - j\xi_{k,M}}]^T =$$

$$[e^{j\eta_{k,1} - j\xi_{k,1}}, \dots, e^{j\eta_{k,M/2} - j\xi_{k,M/2}}, e^{-j\eta_{k,1} - j\xi_{k,1}}, \dots, e^{-j\eta_{k,M/2} - j\xi_{k,M/2}}]^T \quad (9)$$

Evidently, the steering vector of UCA is given by

$$\mathbf{a}(\eta, \xi) = \frac{1}{2} \mathbf{\Psi}(\eta) \mathbf{b}(\xi) = \frac{1}{2} \begin{bmatrix} e^{j\eta_1} & 0 & \dots & 0 & e^{j\eta_1} & 0 & \dots & 0 \\ 0 & e^{j\eta_2} & \ddots & \vdots & 0 & e^{j\eta_2} & \ddots & \vdots \\ \vdots & \ddots & \ddots & 0 & \vdots & \ddots & \ddots & 0 \\ 0 & \dots & 0 & e^{j\eta_{M/2}} & 0 & \dots & 0 & e^{j\eta_{M/2}} \\ e^{-j\eta_1} & 0 & \dots & 0 & e^{-j\eta_1} & 0 & \dots & 0 \\ 0 & e^{-j\eta_2} & \ddots & \vdots & 0 & e^{-j\eta_2} & \ddots & \vdots \\ \vdots & \ddots & \ddots & 0 & \vdots & \ddots & \ddots & 0 \\ 0 & \dots & 0 & e^{-j\eta_{M/2}} & 0 & \dots & 0 & e^{-j\eta_{M/2}} \end{bmatrix} \times \begin{bmatrix} e^{-j\xi_1} \\ e^{-j\xi_2} \\ \vdots \\ e^{-j\xi_{M/2}} \\ e^{-j\xi_1} \\ e^{-j\xi_2} \\ \vdots \\ e^{-j\xi_{M/2}} \end{bmatrix} \quad (10)$$

Note that the $M \times M$ dimensional matrix $\mathbf{\Psi}(\eta)$ in (10) is associated with the 2-D DOA of NFS and does not contain the range parameter.

3. Proposed DIDE method

In this section, the DIDE method is presented to realize

the localization of incoherent signals. Specifically, partial derivative and the LS solution are respectively exploited to acquire the 2-D DOA spatial spectrum and range spatial spectrum. Considering that the partial derivative method needs to utilize the noise subspace, we adapt the propagator to acquire noise subspace, which can reduce computational cost. Due to the fact that the proposed DIDE algorithm does not need the search process for range spatial spectrum, the computational complexity can be significantly reduced.

3.1 Propagator for noise subspace

Considering that the steering vector and the noise subspace of NFS are orthogonal, we first adapt the propagator in [51,53,54] to obtain the noise subspace. The received data of UCA in (7) is divided as

$$\mathbf{X} = \begin{bmatrix} \mathbf{X}_1 \\ \mathbf{X}_2 \end{bmatrix} \quad (11)$$

where $\mathbf{X}_1 \in \mathbf{C}^{K \times N}$ denotes the first row to the K th row of the received data in matrix form, and $\mathbf{X}_2 \in \mathbf{C}^{(M-K) \times N}$ denotes the $(K+1)$ th row to the M th row of the received data in matrix form.

Define the propagator \mathbf{P} satisfying

$$\mathbf{P}^H \mathbf{X}_1 = \mathbf{X}_2. \quad (12)$$

Thus, we can obtain

$$\begin{bmatrix} \mathbf{P}^H & -\mathbf{I}_{M-K} \end{bmatrix} \begin{bmatrix} \mathbf{X}_1 \\ \mathbf{X}_2 \end{bmatrix} = \mathbf{0}_{(M-K) \times N} \quad (13)$$

where \mathbf{I}_{M-K} denotes the $(M-K) \times (M-K)$ dimensional identity matrix and $\mathbf{0}_{(M-K) \times N}$ denotes the $(M-K) \times N$ dimensional zero matrix. By employing the LS method, the propagator \mathbf{P} can be calculated as

$$\hat{\mathbf{P}} = (\mathbf{X}_1 \mathbf{X}_1^H)^{-1} \mathbf{X}_1 \mathbf{X}_2^H. \quad (14)$$

Define the $M \times (M-K)$ dimensional matrix \mathbf{U} as

$$\mathbf{U} = \begin{bmatrix} \hat{\mathbf{P}}^H & -\mathbf{I}_{M-K} \end{bmatrix}^H. \quad (15)$$

Thus, based on (15) and (13), we can obtain

$$\begin{aligned} \mathbf{U}^H \mathbf{X} &= \begin{bmatrix} \hat{\mathbf{P}}^H & -\mathbf{I}_{M-K} \end{bmatrix} \begin{bmatrix} \mathbf{X}_1 \\ \mathbf{X}_2 \end{bmatrix} = \begin{bmatrix} \hat{\mathbf{P}}^H & -\mathbf{I}_{M-K} \end{bmatrix} \begin{bmatrix} \mathbf{A}_1 \mathbf{S} \\ \mathbf{A}_2 \mathbf{S} \end{bmatrix} = \\ & \begin{bmatrix} \hat{\mathbf{P}}^H & -\mathbf{I}_{M-K} \end{bmatrix} \begin{bmatrix} \mathbf{A}_1 \\ \mathbf{A}_2 \end{bmatrix} \mathbf{S} = \mathbf{U}^H \mathbf{A} \mathbf{S} = \mathbf{0}_{(M-K) \times N} \end{aligned} \quad (16)$$

where \mathbf{X}_1 and \mathbf{X}_2 denote the matrices in (11).

Since the matrix $\mathbf{S} \in \mathbf{C}^{K \times N}$ can be partitioned into several $K \times K$ dimensional matrices belonging to invertible matrices, we can further conclude that

$$\mathbf{U}^H \mathbf{A} = \mathbf{0}_{(M-K) \times K}. \quad (17)$$

It can be noticed that matrix \mathbf{U} and steering matrix \mathbf{A} hold the orthogonal property, and matrix \mathbf{U} can be regarded as the noise subspace for the NFS. Note that the partition dimension of propagation operator in (11) is based on the number of signal sources. If we do not know the number of signal sources, we can utilize the detection criterion of the minimum description length (MDL) or Akaike information criterion (AIC) to acquire the number of signals in advance. Moreover, we can calculate the covariance matrix and apply the eigenvalue decomposition (EVD) to acquire the number of signal sources, where the number of signals corresponds to the number of larger eigenvalues. However, calculating the eigenvalues requires additional computational cost.

3.2 Partial derivative for 2-D DOA estimation

In this subsection, we exploit the orthogonal property of the noise subspace \mathbf{U} and the steering vector of UCA to acquire the spatial spectrum of NFS. Based on the 3-D MUSIC method in [40], the 3-D spatial spectrum of NFS is given by

$$\begin{aligned} f(\phi, \theta, r) &= (\mathbf{a}^H(\psi, \xi) \mathbf{U} \mathbf{U}^H \mathbf{a}(\psi, \xi))^{-1} = \\ & (0.25 \mathbf{b}^H(\xi) \mathbf{\Psi}^H(\eta) \mathbf{U} \mathbf{U}^H \mathbf{\Psi}(\eta) \mathbf{b}(\xi))^{-1} = \\ & (0.25 \mathbf{b}^H(\xi) \mathbf{Q}(\eta) \mathbf{b}(\xi))^{-1}. \end{aligned} \quad (18)$$

Obviously, the matrix $\mathbf{Q}(\eta)$ is related to the 2-D DOA and independent of the range parameter of NFS. Obviously, the matrix $\mathbf{Q}(\eta)$ is a Hermite matrix. Thus, the 3-D spatial spectrum function in (18) can be considered as an optimization problem with the objective function being expressed as

$$\begin{aligned} \min & 0.25 \mathbf{b}^H(\xi) \mathbf{Q}(\eta) \mathbf{b}(\xi) \\ \text{s.t.} & \boldsymbol{\rho}^H \mathbf{b}(\xi) = 0 \end{aligned} \quad (19)$$

where $\boldsymbol{\rho} = [1, 0, \dots, 0, -1, 0, \dots, 0]^T$ stands for an $M \times 1$ dimensional constraint vector. The first and the $(M/2+1)$ th elements of $\boldsymbol{\rho}$ are respectively set as 1 and -1 . Define the cost function $L(\eta, \xi)$ as

$$L(\eta, \xi) = 0.25 \mathbf{b}^H(\xi) \mathbf{Q}(\eta) \mathbf{b}(\xi) + \varepsilon \boldsymbol{\rho}^H \mathbf{b}(\xi) \quad (20)$$

where ε is a constant. According to the matrix differentiation in [46]. The partial derivative of the cost function $L(\eta, \xi)$ in (20) versus decomposed vector $\mathbf{b}(\xi)$ is given by

$$\frac{\partial L(\eta, \xi)}{\partial \mathbf{b}(\xi)} = \frac{\partial (0.25 \mathbf{b}^H(\xi) \mathbf{Q}(\eta) \mathbf{b}(\xi))}{\partial \mathbf{b}(\xi)} + \frac{\partial (\varepsilon \boldsymbol{\rho}^H \mathbf{b}(\xi))}{\partial \mathbf{b}(\xi)}. \quad (21)$$

According to the derivation rule of the cross product to

the column vector, the second term in (21) can be expressed as

$$\frac{\partial (\varepsilon \rho^H \mathbf{b}(\xi))}{\partial \mathbf{b}(\xi)} = \varepsilon \frac{\partial (\rho^H \mathbf{b}(\xi))}{\partial \mathbf{b}(\xi)} = \varepsilon \left(\frac{\partial \rho^H}{\partial \mathbf{b}(\xi)} \mathbf{b}(\xi) + \frac{\partial \mathbf{b}^H(\xi)}{\partial \mathbf{b}(\xi)} \rho \right) = \varepsilon (\mathbf{0} \times \mathbf{b}(\xi) + \mathbf{I} \rho) = \varepsilon \rho. \quad (22)$$

Since it is difficult to directly determine the partial derivative of the first term in (21), we analyze the dimensions of the matrix to obtain the result. Exploiting the inexact product rule, the first term in (21) can be expressed as

$$\frac{\partial (0.25 \mathbf{b}^H(\xi) \mathbf{Q}(\eta) \mathbf{b}(\xi))}{\partial \mathbf{b}(\xi)} = 0.25 \frac{\partial (\mathbf{b}^H(\xi) \mathbf{Q}(\eta) \mathbf{d}(\xi))}{\partial \mathbf{b}(\xi)}. \quad (23)$$

Hence, we divide (23) into

$$0.25 \frac{\partial \mathbf{d}(\xi)}{\partial \mathbf{b}(\xi)} = 0.25 \mathbf{I}, \quad (24)$$

and

$$0.25 \frac{\partial (\mathbf{b}^H(\xi) \mathbf{Q}(\eta))}{\partial \mathbf{b}(\xi)} = 0.25 \left(\frac{\partial \mathbf{b}^H(\xi)}{\partial \mathbf{b}(\xi)} \mathbf{Q}(\eta) + \frac{\partial \mathbf{Q}^H(\eta)}{\partial \mathbf{b}(\xi)} \mathbf{b}(\xi) \right) = 0.25 (\mathbf{I} \mathbf{Q}(\eta) + \mathbf{0} \times \mathbf{b}(\xi)) = 0.25 \mathbf{Q}(\eta). \quad (25)$$

By applying dimensional analysis, we can obtain

$$\begin{aligned} 0.25 \frac{\partial (\mathbf{b}^H(\xi) \mathbf{Q}(\eta) \mathbf{d}(\xi))}{\partial \mathbf{b}(\xi)} &= 0.25 \frac{\partial (\mathbf{b}^H(\xi) \mathbf{Q}(\eta)) \mathbf{d}(\xi)}{\partial \mathbf{b}(\xi)} = \\ 0.25 \frac{\partial (\mathbf{b}^H(\xi) \mathbf{Q}(\eta))}{\partial \mathbf{b}(\xi)} \mathbf{d}(\xi) + 0.25 \frac{\partial \mathbf{d}^H(\xi)}{\partial \mathbf{b}(\xi)} \mathbf{Q}^H(\eta) \mathbf{b}(\xi) &= \\ 0.25 \mathbf{Q}(\eta) \mathbf{d}(\xi) + 0.25 \mathbf{I} \mathbf{Q}^H(\eta) \mathbf{b}(\xi). \end{aligned} \quad (26)$$

Therefore, after comparing the dimensions, we can acquire

$$\frac{\partial (0.25 \mathbf{b}^H(\xi) \mathbf{Q}(\eta) \mathbf{b}(\xi))}{\partial \mathbf{b}(\xi)} = 0.25 (\mathbf{Q}(\eta) + \mathbf{Q}^H(\eta)) \mathbf{b}(\xi). \quad (27)$$

Due to the fact that $\mathbf{Q}(\eta)$ is a Hermite matrix, we can utilize the property $\mathbf{Q}(\eta) = \mathbf{Q}^H(\eta)$ to further obtain

$$\frac{\partial (0.25 \mathbf{b}^H(\xi) \mathbf{Q}(\eta) \mathbf{b}(\xi))}{\partial \mathbf{b}(\xi)} = 0.5 \mathbf{Q}(\eta) \mathbf{b}(\xi). \quad (28)$$

Finally, the partial derivative of cost function $L(\eta, \xi)$ in (20) versus decomposed vector $\mathbf{b}(\xi)$ can be expressed as

$$\frac{\partial L(\eta, \xi)}{\partial \mathbf{b}(\xi)} = 0.5 \mathbf{Q}(\eta) \mathbf{b}(\xi) + \varepsilon \rho. \quad (29)$$

Unfortunately, since the rank of angle subspace $\mathbf{Q}(\eta) \in \mathbf{C}^{M \times M}$ is $M/2$, $\mathbf{Q}(\eta)$ does not belong to an invertible matrix. By implementing the pseudo inverse of $\mathbf{Q}(\eta)$, the decomposed vector $\mathbf{b}(\xi)$ can be expressed by

$$\mathbf{b}(\xi) = -2\varepsilon \mathbf{Q}^\dagger(\eta) \rho \quad (30)$$

where $(\cdot)^\dagger$ denotes the pseudo inverse operator.

Since $\mathbf{b}^H(\xi) \mathbf{b}(\xi) = M$, we can obtain

$$4\varepsilon^2 \rho^H \mathbf{Q}^\dagger(\eta) \mathbf{Q}^\dagger(\eta) \rho = M. \quad (31)$$

Hence, the constant ε can be expressed as

$$\varepsilon = \frac{\sqrt{M}}{2 \sqrt{\rho^H \mathbf{Q}^\dagger(\eta) \mathbf{Q}^\dagger(\eta) \rho}}. \quad (32)$$

Then, by inserting (32) into (30), we have

$$\mathbf{b}(\xi) = -\frac{\sqrt{M} \mathbf{Q}^\dagger(\eta) \rho}{\sqrt{\rho^H \mathbf{Q}^\dagger(\eta) \mathbf{Q}^\dagger(\eta) \rho}}. \quad (33)$$

Evidently, by substituting (33) into (19), the spatial spectrum for estimating the 2-D DOA of NFS signals can be acquired by applying the following optimization problem:

$$\begin{aligned} \hat{\eta} &= \arg \min_{\eta} \frac{M \rho^H \mathbf{Q}^\dagger(\eta) \mathbf{Q}(\eta) \mathbf{Q}^\dagger(\eta) \rho}{\text{abs}(\rho^H \mathbf{Q}^\dagger(\eta) \mathbf{Q}^\dagger(\eta) \rho)} = \\ &= \arg \max_{\eta} \frac{\text{abs}(\rho^H \mathbf{Q}^\dagger(\eta) \mathbf{Q}^\dagger(\eta) \rho)}{M \rho^H \mathbf{Q}^\dagger(\eta) \mathbf{Q}(\eta) \mathbf{Q}^\dagger(\eta) \rho}. \end{aligned} \quad (34)$$

Therefore, the spectrum peaks in (34) corresponds to the estimation of 2-D DOA $(\hat{\phi}_k, \hat{\theta}_k)$.

3.3 LS method for range estimation

Considering that searching for the peaks of range spatial spectrum require high computational cost, we exploit the LS method to estimate the range parameter of NFS. Based on (33) and the estimated 2-D DOA $(\hat{\phi}_k, \hat{\theta}_k)$, the decomposed vector $\hat{\mathbf{b}}(\hat{\xi}_k)$ in (33) can be calculated as

$$\hat{\mathbf{b}}(\hat{\xi}_k) = -\frac{\sqrt{M} \hat{\mathbf{Q}}^\dagger(\hat{\eta}_k) \rho}{\sqrt{\rho^H \hat{\mathbf{Q}}^\dagger(\hat{\eta}_k) \hat{\mathbf{Q}}^\dagger(\hat{\eta}_k) \rho}} \quad (35)$$

and thus the phase of $\hat{\mathbf{b}}(\hat{\xi}_k)$ is

$$\begin{aligned} \hat{\mathbf{g}}_k &= \arg \left(\hat{\mathbf{b}}(\hat{\xi}_k) \right) = \\ \frac{\pi R^2}{\lambda r_k} \left[1 - \hat{\zeta}_{k,1}^2, 1 - \hat{\zeta}_{k,2}^2, \dots, 1 - \hat{\zeta}_{k,M}^2 \right]^T &= \mu_k \mathbf{q} \end{aligned} \quad (36)$$

where $\mathbf{q} = \left[1 - \hat{\zeta}_{k,1}^2, 1 - \hat{\zeta}_{k,2}^2, \dots, 1 - \hat{\zeta}_{k,M}^2 \right]^T$ and $\mu_k = \pi R^2 / \lambda r_k$.

Define the objective function for the phase of $\hat{\mathbf{b}}(\hat{\xi}_k)$ as

$$\min_{\mu_k} \|\mathbf{Z} \delta_k - \hat{\mathbf{g}}_k\|_F^2 \quad (37)$$

where the vector δ_k is determined by $[\sigma_k, \mu_k]^T$ and σ_k denotes the error. Moreover, the direction matrix \mathbf{Z} can be expressed as

$$\mathbf{Z} = \begin{bmatrix} 1 & 1 & \dots & 1 \\ 1 - \hat{\zeta}_{k,1}^2 & 1 - \hat{\zeta}_{k,2}^2 & \dots & 1 - \hat{\zeta}_{k,M}^2 \end{bmatrix}^T. \quad (38)$$

Therefore, the LS solution of the vector $\hat{\delta}_k$ can be cal-

culated as

$$\hat{\delta}_k = (\mathbf{Z}^T \mathbf{Z})^{-1} \mathbf{Z}^T \hat{\mathbf{g}}_k. \quad (39)$$

Finally, based on the second element $\hat{\mu}_k$ in $\hat{\delta}_k$, the estimation for the paired range parameter can be obtained as

$$\hat{r}_k = \frac{\pi R^2}{\lambda \hat{\mu}_k}. \quad (40)$$

Fig. 2 displays the flow chart of the proposed DIDE method. Note that if the estimation of range parameter exceeds the near-field area of UCA, the k th signal should be regarded as an FFS.

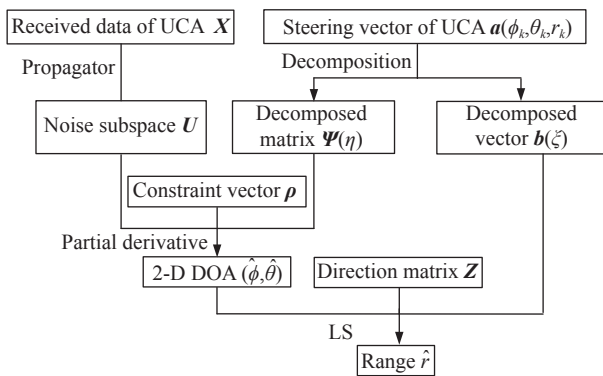


Fig. 2 Flow chart of the proposed DIDE method

3.4 Analysis of computational cost

As for the computational complexity of proposed DIDE method, the propagator in (13) requires $O(K^2N + KMN)$ calculation, the matrix $\mathbf{Q}(\eta)$ in (18) requires $O((M^2 + 2M)(M - K))$ calculation, the 2-D DOA search process in (26) needs $O((360 \times 90 / \Delta_{\text{DOA}}^2)(10M + M^2))$ calculation, and that of performing LS method for range estimation in (31) is $O(13M)$, where Δ_{DOA} stands for the interval of 2-D DOA spatial spectrum. Noticeably, the proposed DIDE algorithm can acquire the range parameter without searching for the peaks of range spatial spectrum.

4. Computer simulation results

In this section, 16 sensors with radius $R=1$ m form the configuration of UCA. We first verify the effectiveness of the proposed DIDE method for near-field source localization. Then, the computational cost and root mean square error (RMSE) are compared with that of the TSMUSIC method in [41], the SOS-based method in [42] and the phase-based method in [45]. Moreover, based on whether the calculated range parameter is in the near-field area of UCA, we apply the proposed DIDE algorithm to classify of the mixed NFSs and FFSs.

4.1 Effectiveness of location

In the simulation, two NFS are respectively located at $(30^\circ, 50^\circ, 10 \text{ m})$ and $(60^\circ, 20^\circ, 5 \text{ m})$. The wavelength of signal is 0.3 m and the interval of 2-D DOA spatial spectrum is set as 0.1° . The 2-D DOA spatial spectrum obtained by the proposed partial derivative method is shown in Fig. 3, where the signal-to-noise ratio (SNR) is set as 20 dB and the number of snapshot is set as 2 000. It can be noticed that the spectrum peaks correspond to the 2-D DOA of the mentioned NFS.

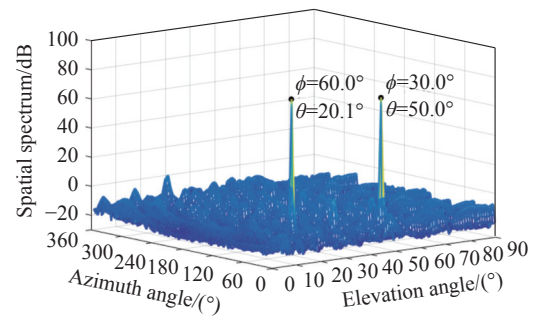


Fig. 3 2-D DOA spatial spectrum

Based on the estimated 2-D DOA, the range parameter of NFS are computed by applying the LS method, Fig. 4 displays the result of 3-D localization, where the red dots and + shaped marks denote the estimated locations and real locations of the mentioned signals respectively. We can conclude that the estimated 3-D parameters are automatically paired and the proposed DIDE method can realize near-field source localization.

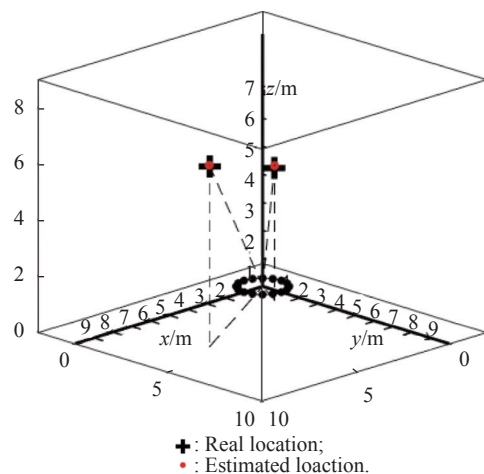


Fig. 4 3-D location result of two NFS

4.2 Comparison of computational cost

In order to further illustrate and discuss the performance,

the computational complexity of proposed DIDE algorithm is compared with that of the TSMUSIC method in [41], the SOS-based method in [42], and the phase-based method in [45]. By transforming 3-D localization into 2-D and 1-D parameter estimation, the TSMUSIC method and SOS-based method respectively utilize 2-D MUSIC and ESPRIT-like to estimate 2-D DOA. Yet, both TSMUSIC method and SOS-based method employ 1-D MUSIC to acquire the range parameters of near-field sources. In contrast, the proposed DIDE algorithm can acquire the range parameter without searching for the peaks of range spatial spectrum. Table 1 displays the computational complexity of the above-mentioned methods.

Table 1 Computational complexity comparison

Algorithm	Computational complexity
DIDE	$O(K^2M + KMN + (M^2 + 2M)(M - K) + (360 \times 90 / \Delta_{\text{DOA}}^2) \cdot (M^2 + 10M) + 13M)$
TSMUSIC	$O(M(N-1)/2 + M^2N + 2M^3 + (360 \times 90 / \Delta_{\text{DOA}}^2)(M + 2M^2) + K((8R^2/\lambda - 0.62(8R^3/\lambda)^{1/2})/\Delta_{\text{range}})(M + 2M^2))$
SOS-based	$O(M^2N + M^3 + 2K^2M(360 \times 90 / \Delta_{\text{DOA}}^2) + K((8R^2/\lambda - 0.62(8R^3/\lambda)^{1/2})/\Delta_{\text{range}})(M + 2M^2))$
Phase-based	$O(KNM + 20KM)$

With regard to the time cost, the elapsed CPU time of aforementioned methods are compared in the simulation. As a result, the time consuming of the proposed DIDE algorithm, the TSMUSIC algorithm, the SOS-based algorithm, and the phase-based algorithm are 0.65 s, 1.16 s, 0.81 s, and 0.22 s, respectively. Similarly, we can conclude that the proposed DIDE algorithm is more computationally efficient than the TSMUSIC method and the SOS-based method.

4.3 RMSE comparison of near-field sources

In this subsection, RMSE is utilized to verify the performance of the proposed DIDE algorithm, which is calculated as

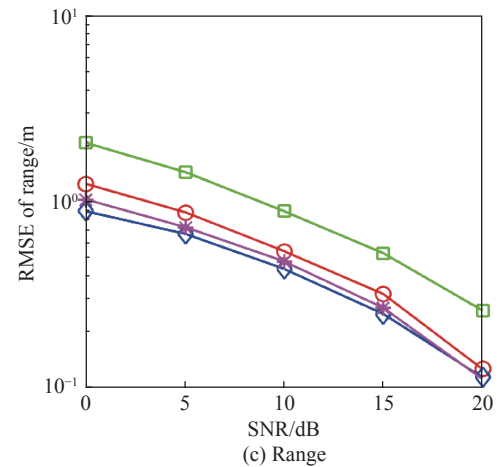
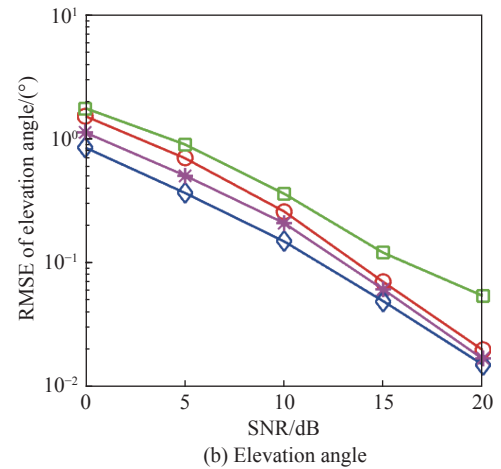
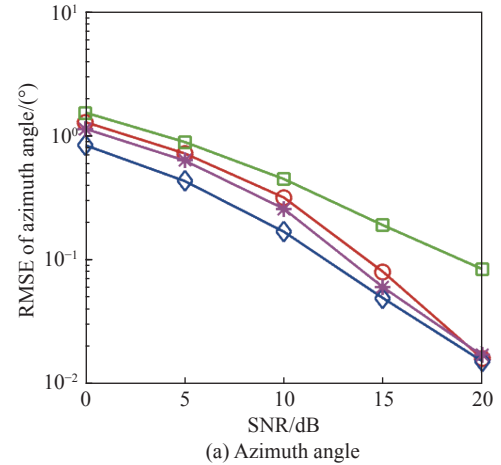
$$\text{RMSE}(\beta) = \sqrt{\frac{1}{KV} \sum_{k=1}^K \sum_{v=1}^V (\hat{\beta}_{k,v} - \beta_k)^2},$$

$$k = 1, 2, \dots, K; \quad v = 1, 2, \dots, V \quad (41)$$

where K denotes the number of signals, V denotes the number of Monte-Carlo simulations, $\hat{\beta}_{k,v}$ denotes the estimation of 3-D location parameter $(\hat{\phi}, \hat{\theta}, \hat{r})$ of the k th signal in the v th Monte-Carlo simulation, and β_k denotes the actual 3-D location parameters (ϕ, θ, r) of the k th signal.

The RMSEs versus SNRs from 0 dB to 20 dB are given in Fig. 5(a)–Fig. 5(c), where the number of Monte-Carlo simulations is set to 500 and the number of snap-

shot is set to 2 000. Thus, we can conclude that the 3-D parameter estimation accuracy of the proposed DIDE method is higher than that of the phase-based method and can be close to that of the SOS-based method at higher SNR.



Legend:
○ : Proposed algorithm; ✱ : SOS-based method;
◇ : TSMUSIC method; □ : Phase-based method.

Fig. 5 RMSEs versus SNRs

With regards to the resolution probability, we compare the estimation successful probability versus the SNR, where the estimation successful probability at each SNR is calculated by the ratio between the number of successful simulations and the number of total simulations. Fig. 6 displays the estimation successful probability from -20 dB to 10 dB, where the two NFS are located at $(30^\circ, 50^\circ, 10 \text{ m})$ and $(33^\circ, 53^\circ, 13 \text{ m})$, the number of Monte-Carlo simulations and snapshot are set as 500 and $2\,000$, respectively. It can be noticed that the estimation successful probability improves as the value of SNR increases. Moreover, the estimation successful ability of the proposed DIDE method is better than that of SOS-based and phased-based methods especially in the case of low SNR.

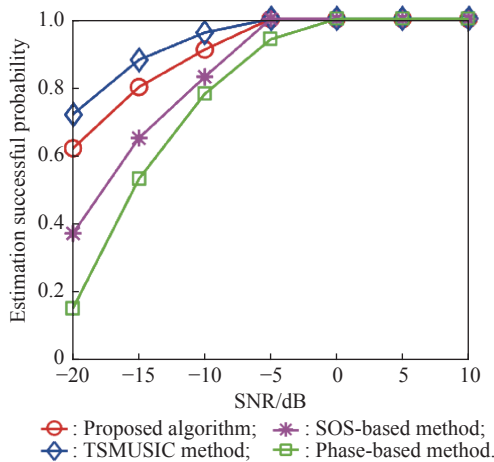


Fig. 6 Estimation successful probability versus SNR

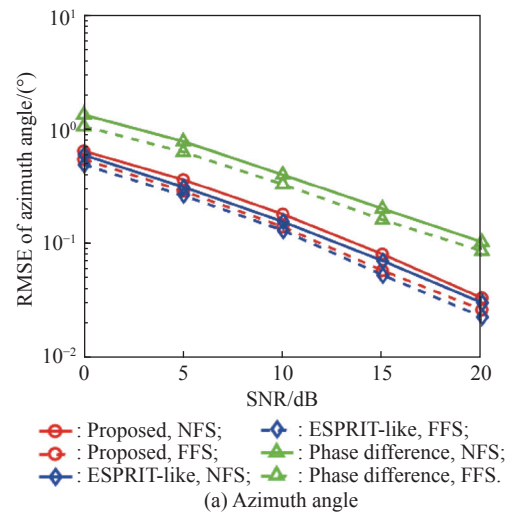
4.4 RMSE comparison of mixed sources

In this subsection, we execute an RMSE under the scenario of mixed NFSs and FFSs. Based on whether the calculated range parameter is in the near-field area of the UCA, we achieve the classification of the mixed sources. To be exact, if the calculated range value is in the near-field region of the UCA, the signal is regarded as an NFS. Conversely, if the calculated range value exceeds the near-field region of the UCA, the signal is considered as an FFS.

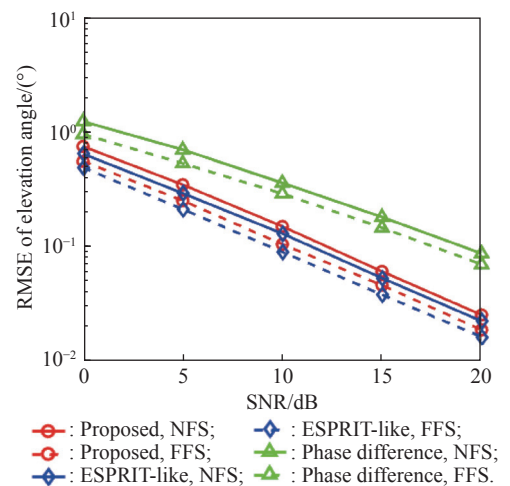
By utilizing the configuration of UCA to achieve mixed sources localization, the RMSE of the proposed DIDE algorithm is compared with that of ESPRIT-like algorithm in [51] and phase difference algorithm in [52]. The algorithm in [51] exploits the configuration of UCA and utilizes the covariance differencing method to decouple pure NFSs. Then, the improved ESPRIT-like method and 1-D MUSIC method are respectively applied to obtain 2-D DOA spatial spectrum and range spatial spectrum. The algorithm in [52] utilizes the phase difference of the centro-symmetric sensors to separate 2-D DOA and range parameter. Then, the closed-form method and

1-D MUSIC method are respectively performed to acquire 2-D DOA and range parameter. Finally, if there is a peak in the range spatial spectrum, the signal can be considered as an NFS and the spectrum peak is corresponding to range parameter. By contrary, if the range spatial spectrum is not convergent, the signal can be regarded as an FFS.

The RMSEs versus SNRs from 0 dB to 20 dB are given in Fig. 7(a)–Fig. 7(c), where the NFS and the FFS are respectively located at $(30^\circ, 50^\circ, 10 \text{ m})$ and $(60^\circ, 20^\circ, \infty)$, the number of snapshot and Monte-Carlo simulations are respectively set as $2\,000$ and 500 . Noticeably, as the SNR increases, the RMSE of the proposed DIDE algorithm gradually decreases. Since the signal model of the NFS is simplified, it is affected by the error of Taylor series expansion. However, the signal model for the NFS is not simplified, the estimation accuracy of FFS is more accurate than that of NFS. Moreover, in comparison to the phase difference algorithm, the proposed DIDE algorithm can obtain higher estimation accuracy of mixed signals.



(a) Azimuth angle



(b) Elevation angle

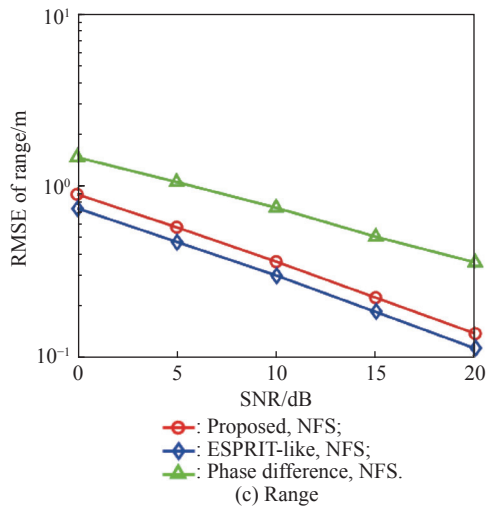


Fig. 7 RMSE versus SNR

5. Conclusions

In this paper, we present a DIDE algorithm to realize the localization of incoherent signals via the geometry of UCA. We respectively exploit propagator, partial derivative and LS method to obtain noise subspace, 2-D DOA spatial spectrum and range parameter. The proposed DIDE method can determine range parameter without the searching process of the spatial spectrum, which is more computationally efficient than the TSMUSIC method and SOS-based method. Moreover, the 3-D parameter estimation accuracy of the proposed DIDE method is higher than that of the phase-based method. Furthermore, we employ the proposed DIDE algorithm to classify the mixed incoherent NFSs and FFSs. In comparison to the phase difference algorithm, the proposed DIDE algorithm can obtain higher estimation accuracy of mixed signals.

References

- [1] ZHANG Y, HE P Y, PAN F. Three-dimension localization of wideband sources using sensor network. *Chinese Journal of Electronics*, 2017, 26(6): 1302–1307.
- [2] SHI J P, WEN F Q, LIU T P. Nested MIMO radar: coarrays, tensor modeling, and angle estimation. *IEEE Trans. on Aerospace and Electronic Systems*, 2021, 57(1): 573–585.
- [3] LIANG J L, LIU D. Passive localization of near-field sources using cumulant. *IEEE Sensors Journal*, 2009, 9(8): 953–960.
- [4] HE J, SWAMY M N S, AHMAD M O. Efficient application of MUSIC algorithm under the coexistence of far-field and near-field sources. *IEEE Trans. on Signal Processing*, 2012, 60(4): 2066–2070.
- [5] LIU G, SUN X Y. Spatial differencing method for mixed far-field and near-field sources localization. *IEEE Signal Processing Letters*, 2014, 21(11): 1331–1335.
- [6] GAZZAH H, DELMAS J P. CRB-based design of linear antenna arrays for near-field source localization. *IEEE Trans. on Antennas and Propagation*, 2014, 62(4): 1965–1974.
- [7] SHI J P, HU G P, ZHANG X F, et al. Sparsity-based DOA estimation of coherent and uncorrelated targets with flexible MIMO radar. *IEEE Trans. on Vehicular Technology*, 2019, 68(6): 5835–5848.
- [8] KUMAR L, HEGDE R M. Near-field acoustic source localization and beamforming in spherical harmonics domain. *IEEE Trans. on Signal Processing*, 2016, 64(13): 3351–3361.
- [9] SINGH P R, WANG Y D, CHARGE P. A correction method for the near-field approximated model based localization techniques. *Digital Signal Processing*, 2017, 67: 76–80.
- [10] SU X L, LIU Z, SUN B, et al. Fast BSC-based algorithm for near-field signal localization via uniform circular array. *Journal of Systems Engineering and Electronics*, 2022, 33(2): 269–278.
- [11] QIAN T, CUI W, SHEN Q. Sparse reconstruction method for DOA estimation based on dynamic dictionary and negative exponent penalty. *Chinese Journal of Electronics*, 2018, 27(2): 386–392.
- [12] SHAN T J, WAX M, KAILATH T. On spatial smoothing for direction-of-arrival estimation coherent signal. *IEEE Trans. on Acoustics, Speech, and Signal Processing*, 1985, 37(1): 8–15.
- [13] MALIOUTOV D, CETIN M, WILLSKY A S. A sparse signal reconstruction perspective for source localization with sensor arrays. *IEEE Trans. on Signal Processing*, 2005, 53(8): 3010–3022.
- [14] XU J W, WANG B, HU F Y. Near-field sources localization in partly calibrated sensor arrays with unknown gains and phases. *IEEE Wireless Communications Letters*, 2018, 8(1): 89–92.
- [15] ZUO W L, XIN J M, ZHENG N N, et al. Subspace-based localization of far-field and near-field signals without eigen-decomposition. *IEEE Trans. on Signal Processing*, 2018, 66(17): 4461–4476.
- [16] CHEN J C, HUDSON R E, YAO K. Maximum-likelihood source localization and unknown sensor location estimation for wideband signals in the near-field. *IEEE Trans. on Signal Processing*, 2002, 50(8): 1843–1854.
- [17] HUANG Y D, BARKAT M. Near-field multiple source localization by passive sensor array. *IEEE Trans. on Antennas and Propagation*, 1991, 9(7): 968–975.
- [18] WEISS A J, FRIEDLANDER B. Range and bearing estimation using polynomial rooting. *IEEE Journal of Oceanic Engineering*, 1993, 18(2): 130–137.
- [19] ARSLAN G, SAKARYA F A. A unified neural-network-based speaker localization technique. *IEEE Trans. on Neural Network*, 2000, 11(4): 997–1002.
- [20] ZHI W, CHIA M Y W. Near-field source localization via symmetric subarrays. *IEEE Signal Processing Letters*, 2007, 14(6): 409–412.
- [21] ZHENG Z, FU M C, WANG W Q, et al. Localization of mixed near-field and far-field sources using symmetric double-nested arrays. *IEEE Trans. on Antennas and Propagation*, 2019, 67(11): 7059–7070.
- [22] STARER D, NEHORAI A. Passive localization of near-field sources by path following. *IEEE Trans. on Signal Processing*, 1994, 42(3): 677–680.
- [23] LEE J H, LEE C M, LEE K K. A modified path-following algorithm using a known algebraic path. *IEEE Trans. on Signal Processing*, 1999, 47(5): 1407–1409.
- [24] LEE J H, CHEN Y M, YEH C C. A covariance approximation method for near-field direction-finding using a uniform

- linear array. *IEEE Trans. on Signal Processing*, 1995, 43(5): 1293–1298.
- [25] NOH H, LEE C. A covariance approximation method for near-field coherent sources localization using uniform linear array. *IEEE Journal of Oceanic Engineering*, 2015, 40(1): 187–195.
- [26] YUEN N, FRIEDLANDER B. Performance analysis of higher order ESPRIT for localization of near-field sources. *IEEE Trans. on Signal Processing*, 1998, 46(3): 709–719.
- [27] WU Y T, MA L, HOU C H, et al. Subspace-based method for joint range and DOA estimation of multiple near-field sources. *Signal Processing*, 2006, 86(8): 2129–2133.
- [28] LI J Z, WANG Y D, GANG W. Signal reconstruction for near-field source localisation. *IET Signal Processing*, 2014, 9(3): 201–205.
- [29] ADACHI Y, IIGUNI Y, MAEDA H. Second-order approximation for DOA estimation of near-field sources. *Circuits Systems and Signal Processing*, 2003, 22(3): 287–306.
- [30] KUMAR L, HEGDE R M. Near-field acoustic source localization and beamforming in spherical harmonics domain. *IEEE Trans. on Signal Processing*, 2016, 64(13): 3351–3361.
- [31] PAN J J, SINGH P R, MEN S Y. A search-free near-field source localization method with exact signal model. *Journal of Systems Engineering and Electronics*, 2021, 32(4): 756–763.
- [32] LEE J H, TUNG C H. Estimating the bearings of near-field cyclostationary signals. *IEEE Trans. on Signal Processing*, 2002, 50(1): 110–118.
- [33] FRIEDLANDER B. Localization of signals in the near-field of an antenna array. *IEEE Trans. on Signal Processing*, 2019, 67(15): 3885–3893.
- [34] ZUO W L, XIN J M, LIU W Y, et al. Localization of near-field sources based on linear prediction and oblique projection operator. *IEEE Trans. on Signal Processing*, 2019, 67(2): 415–430.
- [35] CHEN H, WANG W F, LIU W. Joint DOA, range, and polarization estimation for rectilinear sources with a COLD array. *IEEE Wireless Communications Letters*, 2019, 8(5): 1398–1401.
- [36] CHEN H, ZHU W P, LIU W, et al. RARE-based localization for mixed near-field and farfield rectilinear sources. *Digital Signal Processing*, 2019, 85: 54–61.
- [37] LI J Z, WANG Y D, BASTARD C L, et al. Simplified high-order DOA and range estimation with linear antenna array. *IEEE Communications Letters*, 2017, 21(1): 76–79.
- [38] SU X L, LIU Z, CHEN X, et al. Closed-form algorithm for 3-D nearfield OFDM signal localization under uniform circular array. *Sensors*, 2018, 18(1): 226.
- [39] GOOSSENS R, ROGIER H, WERBROUCK S. UCA root-MUSIC with sparse uniform circular arrays. *IEEE Trans. on Signal Processing*, 2008, 56(8): 4095–4099.
- [40] LEE J H, PARK D H, PARK G T, et al. Algebraic path-following algorithm for localising 3-D near-field sources in uniform circular array. *Electronics Letters*, 2003, 39(17): 1283–1285.
- [41] WU Y T, WANG H, ZHANG Y B, et al. Multiple near-field source localisation with uniform circular array. *Electronics Letters*, 2013, 49(24): 1509–1510.
- [42] SU X L, LIU Z, CHEN X, et al. An SOS-based algorithm for localization of multiple near-field sources using uniform circular array. *IEEE Sensors Letters*, 2019, 3(11): 5501004.
- [43] JUNG T J, LEE K K. Closed-form algorithm for 3-D single-source localization with uniform circular array. *IEEE Antennas and Wireless Propagation Letters*, 2014, 13: 1096–1099.
- [44] BOYER E, FERREOL A, LARZABAL P. Simple robust bearing-range source’s localization with curved wavefronts. *IEEE Signal Processing Letters*, 2005, 12(6): 457–460.
- [45] CHEN X, LIU Z Z, WEI X Z. Unambiguous parameter estimation of multiple near-field sources via rotating uniform circular array. *IEEE Antennas and Wireless Propagation Letters*, 2017, 16: 872–875.
- [46] ZHANG X Y, CHEN W Y, ZHENG W, et al. Localization of near-field sources: a reduced-dimension MUSIC algorithm. *IEEE Communications Letters*, 2018, 22(7): 1422–1425.
- [47] TIAN Y, LIAN Q S, XU H. Mixed near-field and far-field source localization utilizing symmetric nested array. *Digital Signal Processing*, 2017, 73: 16–23.
- [48] WANG B, ZHAO Y P, LIU J J. Mixed-order MUSIC algorithm for localization of far-field and near-field sources. *IEEE Signal Processing Letters*, 2013, 20(4): 311–314.
- [49] TIAN Y, WANG Y R, RONG X L, et al. Mixed source localization and gain-phase perturbation calibration in partly calibrated symmetric uniform linear arrays. *Signal Processing*, 2020, 166: 107267.
- [50] JIANG J J, DUAN F J, CHEN J, et al. Mixed near-field and far-field sources localization using the uniform linear sensor array. *IEEE Sensors Journal*, 2013, 13(8): 3136–3143.
- [51] SU X L, LIU Z, LIU T P, et al. Passive localization of mixed near-field and far-field sources without eigendecomposition via uniform circular array. *Circuits Systems and Signal Processing*, 2020, 39(4): 5298–5317.
- [52] SU X L, LIU Z, CHEN X, et al. Mixed incoherent far-field and near-field source localization under uniform circular array. *Sensors*, 2018, 18(5): 1432.
- [53] ZHENG Z, LI G J, TENG Y L. 2D DOA estimator for multiple coherently distributed sources using modified propagator. *Circuits Systems and Signal Processing*, 2012, 31(1): 255–270.
- [54] MUNIER J, DELISLE G Y. Spatial analysis using new properties of the cross-spectral matrix. *IEEE Trans. on Signal Processing*, 1991, 39(3): 746–749.

Biographies



SU Xiaolong was born in 1994. He received his M.S. degree from National University of Defense Technology, Changsha, China, in 2018. He is currently pursuing his Ph.D. degree in National University of Defense Technology. His research interests include array signal processing and deep learning.
E-mail: suxiaolong_nudt@163.com



HU Panhe was born in 1991. He received his Ph.D. degree from National University of Defense Technology, Changsha, China, in 2019. He is an associate professor in National University of Defense Technology. His research interests include radar system design, array signal processing, and deep learning.
E-mail: hupanhe13@nudt.edu.cn



WEI Zhenhua was born in 1983. He received his M.S. degree from National University of Defense Technology, Changsha, China, in 2006. He is an associate professor in Rocket Force University of Engineering. His research interests include anti-jamming and wireless communication.
E-mail: wzh016001@aliyun.com



SHI Junpeng was born in 1988. He received his Ph.D. degree from Air Force Engineering University, Xi'an, China, in 2018. He is an associate professor in National University of Defense Technology. His research interest is tensor signal processing with sparse MIMO radar.
E-mail: shijunpeng20@nudt.edu.cn



LIU Zhen was born in 1983. He received his Ph.D. degree from National University of Defense Technology, Changsha, China, in 2013. He is a professor in National University of Defense Technology. His research interests include radar target recognition and countermeasures, array signal processing and machine learning.
E-mail: zhen_liu@nudt.edu.cn



LI Xiang was born in 1967. He received his Ph.D. degree from National University of Defense Technology, Changsha, China, in 1998. He is a professor in National University of Defense Technology. His research interests include target recognition, signal detection, and radar imaging.
E-mail: lixiang01@vip.sina.com